Characterization of photon-counting detector responsivity for non-linear two-photon absorption process

S. E. Sburlan and W. H. Farr
Jet Propulsion Laboratory, California Institute of Technology, 4800 Oak Grove Dr., Pasadena, CA

ABSTRACT

Sub-band absorption at 1550 nm has been demonstrated and characterized on silicon Geiger mode detectors which normally would be expected to have no response at this wavelength. We compare responsivity measurements to single-photon absorption for wavelengths slightly above the bandgap wavelength of silicon (~1100 μm). One application for this low efficiency sub-band absorption is in deep space optical communication systems where it is desirable to track a 1030 nm uplink beacon on the same flight terminal detector array that monitors a 1550 nm downlink signal for pointing control. The currently observed absorption at 1550 nm provides 60-70 dB of isolation compared to the response at 1064 nm, which is desirable to avoid saturation of the detector by scattered light from the downlink laser.

Keywords: two-photon, Geiger mode detector, optical communications, responsivity, non-linear absorption, microlens array, detection efficiency, pixel

1. INTRODUCTION

Optical communication systems have the potential to provide 10 to 100 times higher data rates from deep space to Earth for a similar spacecraft burden (mass and power) of a microwave RF transmitter[1]. Currently, JPL is studying the Deep-space Optical Terminals (DOT) concept to demonstrate the advantages of such a link between Earth and Mars[2]. The proposed flight terminal design includes a focal-plane-array detector that can simultaneously acquire and track an uplink beacon transmitted from Earth to determine the Earth receiver location, track the pointing of the downlink transmit laser, and detect uplink data modulation. Currently, an effort is underway to demonstrate centroiding and command channel demodulation algorithms in hardware using a 6 x 6 silicon photon-counting Geiger mode array, with planned scaling to 32x32 and larger arrays[3]. Such detectors, offering a larger focal plane area, have the potential to facilitate the initial uplink beacon acquisition phase compared to a traditional quad (2 x 2) array. In addition, multiple pixel arrays can track objects other than the received beacon. For example, the Earth's crescent can also be imaged on such an array in order to serve as a backup mechanism for the uplink beacon and point-ahead calculation in the event that the uplink beacon is temporarily lost.

Both CCD cameras and photon counting detectors have been considered for this application. Photon counting detector arrays can provide a number of advantages over CCDs. Firstly, photon-counting detectors provide a factor of ~10^5 more precision in the time of arrival information for each detected photon, which can be used to detect high MB/s uplink data modulation and for laser ranging experiments. Secondly, they can allow faster read-out speeds than CCDs for higher rate tracking. Lastly, photon-counting detectors have lower read-out noise than CCDs, especially at high frame readout rates. We have previously shown that a photon-counting detector allows centroiding estimates to be calculated with estimation errors close to the theoretical shot noise limit[4]. This serves to reduce the required transmitted power from Earth to acquire and track the uplink beacon. Furthermore, low noise characteristics enable the implementation of high data rate channels on the uplink signal.

Another of DOT's novel approaches outlined in Ref. [5] proposes to implement sub-band gap tracking of a normally invisible transmit laser on the focal plane array. Besides detection of the uplink beacon wavelength, it is necessary to track the outgoing angle of the downlink laser beam as an in-flight calibration mechanism for the laser's pointing

direction towards Earth. The downlink laser has wavelength of 1550 nm, and typically is undetectable by any material with higher corresponding band gap energy. In our prototype model, the silicon Geiger mode detector does not absorb photons with wavelengths below ~1100 nm. Nevertheless, photons with energies below the band gap may be absorbed through a two-photon process[6] in which two low-energy photons that impinge on the detector in close temporal and spatial proximity are absorbed by a single electron that is excited from the valence to the conduction band. Because a tightly focused beam is necessary for this process, and the detection efficiency is inherently lower than direct absorption of photons at the band gap energy and higher, a high isolation factor exists between the uplink and downlink signals[7].

We characterized the two-photon responsivity of individual pixels of a 6 x 6 Geiger mode array that incorporates an active quenching circuit, as well as a passively quenched single pixel photon counting module, and measured a responsivity at 1550 nm that is ~60 dB below that previously measured at 1064 nm. Theoretically, we expect the rate of two-photon absorption to be proportional to the field intensity squared. This can be understood intuitively by considering that the absorption rate depends on the number of photon-pairs in which photons coincide in time and space. Thus, increasing the number of possible photon pairs will increase the probability of absorption. A beam having n photons arriving in a given time interval has $\frac{1}{2}(n^2 - n)$ possible photon pairs. Therefore, doubling n results in a four-fold increase in the possible photon pairs, which will increase the absorption rate accordingly. Nevertheless, to date our measurements with Geiger mode devices has yielded a nearly linear increase in the number of generated pulses with increasing laser power. The linear response is indicative of single photon absorption at 1550 nm, which is possible in the presence of inner-band energy states. Measurements on the single pixel photon counting module also yielded a nearly linear response, but provided evidence of an overlapping quadratic element signaling two-photon absorption.

2. RESULTS AND ANALYSIS

The detector array is positioned at the focal point of a 1550 nm laser beam (Fig. 1a). The array detector construction includes a microlens array made of quartz having 250 µm focal length and fill factor of 75% (Fig. 2a). The microlenses and detector array have the same pitch of 100 µm. Each lens focuses light on the detector with 13µm active area. As Fig. 1b shows, the active area of the detector comprises a 6 x 6 pixel region. The detector's active quenching circuit produces square pulses 3 V in amplitude and 25 ns length for each absorbed photon (Fig. 1c). A logic analyzer and software is used to count the pulses with a sampling rate of 10 ns in time intervals of 2.62 ms. The counts on each pixel can be viewed in real time using customized software. As depicted in Fig. 2b, the total counts on each pixel in 2.62 ms are displayed on a red color scale relative to the maximum number of counts on a single pixel. Using this approach, the observed counts on a given pixel were maximized by finely tuning the position of the detector mounted on a translation stage in the beam's cross-sectional (xy) plane, as well as finding the optimal focusing position along the z axis. As the position is adjusted in xy, we observe individual pixels illuminated in a sequential fashion so that a single pixel appears brightest as shown in Fig. 2b.

To measure the responsivity of an individual pixel as the incident power is increased, we initially adjusted the detector position in x, y, and z so that the counts on pixel 15 are maximized. In this configuration, we measured the total counts captured by the logic analyzer for that pixel in 2.62 msec intervals for 800 trials as the incident power on the detector was adjusted to be between 0 and 1.8 mW. At each power level, the observed counts are averaged over all the trials and the standard deviation is computed. Fig. 3a plots the results showing a linear increase in the number of counts as the incident power is increased. In this case, the responsivity of the pixel appears to be constant and equal to $7.9x10^5$ counts/(s·mW). The previously measured responsivity of the detector at 1064 nm[4] was between $1.72x10^{11}$ and $1.16x10^{12}$. (For incident power of 1.55 nW, total observed counts ranged between 700 and 4700 in 2.62 msec.) In terms of detection efficiency computed from

$$DE = \frac{counts}{photons} = \frac{hc*counts}{P\lambda t},$$

where P, λ are the incident power and wavelength respectively, and t is the time interval in seconds, we find that the detection efficiency is $DE_{\lambda=1550} = 1.01x10^{-10}$ $counts/photon$ and $DE_{\lambda=1064} = 3.22x10^{-5} - 2.1610^{-4}$ $counts/photon$, giving 55 to 63 dB of isolation between the two processes. In

our current experiment using the 1550 nm source, there is no observable response for incident powers below 10 μW on a given pixel whereas previously a few nW of power at 1064 nm could saturate the detector. The smaller responsivity is expected for two-photon absorption compared to the much stronger single photon-process, and serves to validate the DOT conceptual design which would benefit from the ~60 dB of isolation that enables tracking of two wavelengths on a single photon-counting detector. The high isolation factor ensures that stray light from the downlink laser will not saturate the detector.

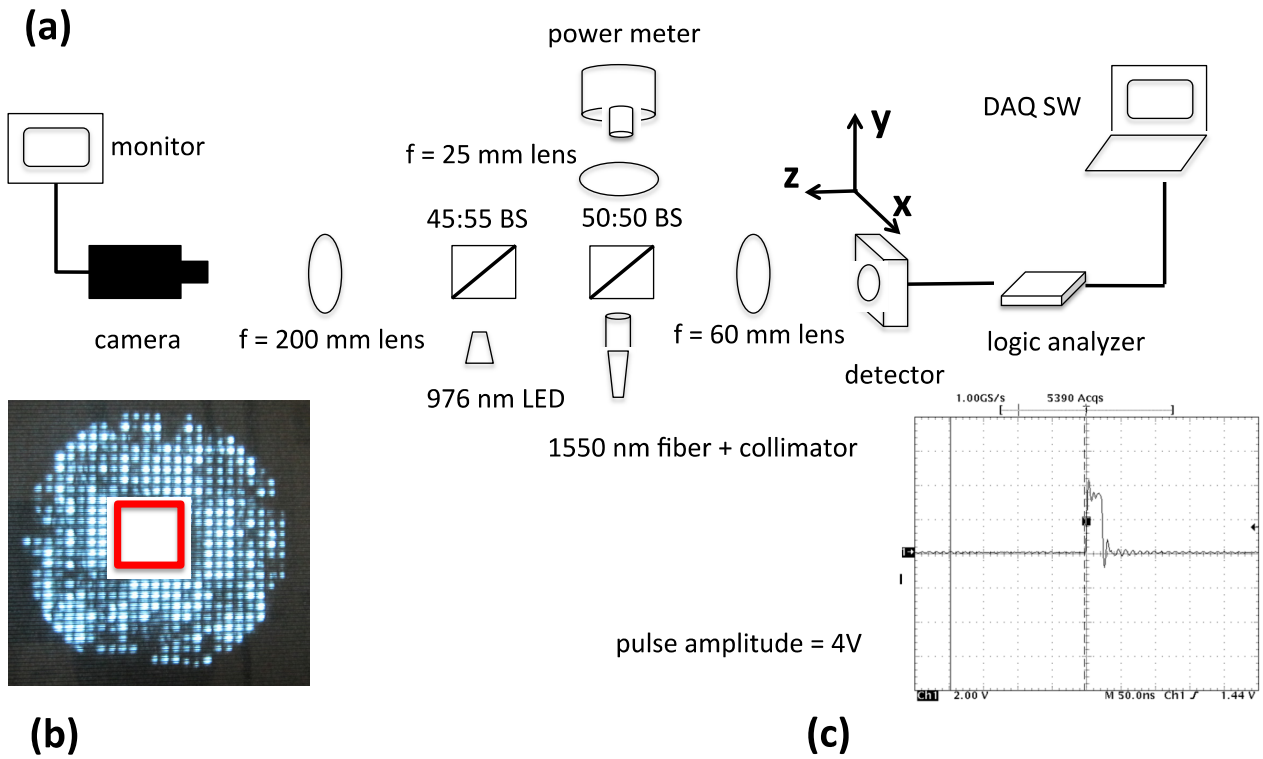

Fig. 1(a) Experimental setup for responsivity measurements on Geiger mode detector. The output of a 1550 nm fiber-coupled laser is collimated and passes through a 50/50 beam splitter to the power meter as well as to the detector via the refocusing lens. The logic analyzer samples the pixel channels at 10 ns intervals, recording zero-crossing transitions as bits onto the PC hard disk. An LED also illuminates the detector, which is imaged onto a camera (b). Red square depicts the active region 6 x 6 pixel array. The detector outputs pulses of 25 ns duration and 4 V amplitude (c).

We observed the same linear increase in counts consistently on multiple pixels in the array. In addition, we monitored the total current drawn by the detector at different power levels and found it to be proportional to the count rate, thereby also increasing linearly with incident power. We have also carried out several tests to confirm that the observed response is indeed due to absorption of photons having 1550 nm wavelength. For the first test, we placed a dichroic mirror in the optical path at a 45° angle from an *xy* plane. At this angle, the mirror reflects 1550 light at 90° from the *z* axis, while passing shorter wavelengths. We verified visually that a 1.8 mW beam of 1550 light was reflected at 90°, and observed that the detector response fell to nearly zero. When the mirror was removed, the pixel once again began to register counts. For the second test, we used a bandpass filter centered at 1530 nm having FWHM = 12 ± 2.4 nm in the optical path. We observed the pixel response decreased significantly, yet still clearly distinguishable above the noise level. Finally, we confirmed using a bandpass filter centered at 1550 nm in the optical path that the response was unchanged as expected. Since the filter blocks all other wavelengths in the range of 200 - 1850 nm, our observations confirm that the response is indeed due to absorption of 1550 nm photons, but the linear response indicates a single

photon rather than two photon interaction below the silicon bandgap energy. This linear dependence of counts on incident power has been previously reported in Ref. [8]. In that work, a constant responsivity was observed below 10 mW of incident power on a silicon PIN photodiode. For higher powers, a quadratic increase in the detector current became apparent.

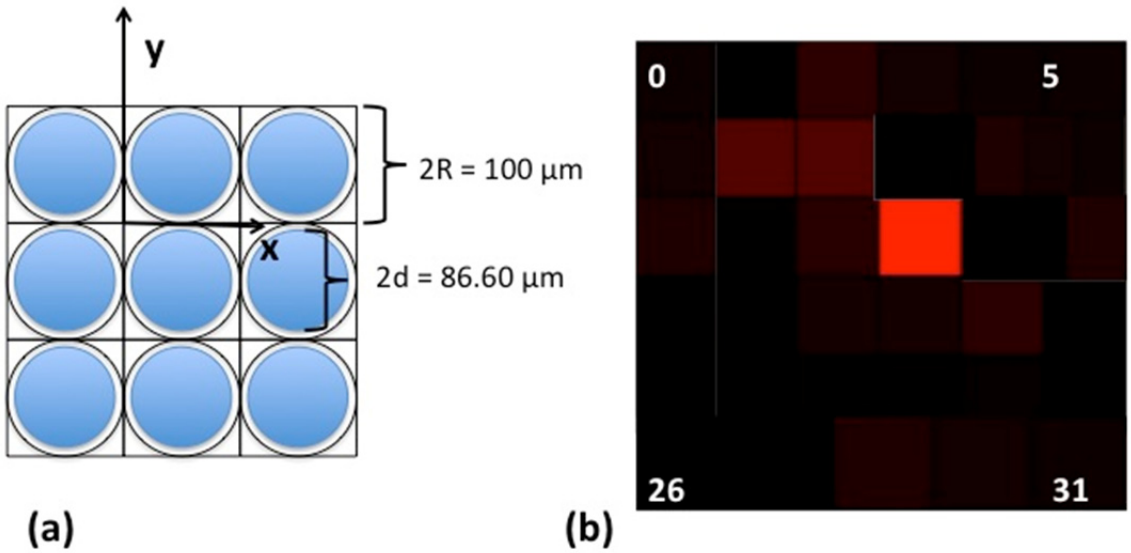

Fig. 2 (a) Geiger mode array with 100 µm quartz microlens system. Each lens has a fill factor of 75% for an effective diameter of 86.6 µm. Only light incident on the shaded region of the lens will be focused on the detector behind it, which has active area of 13 µm. (b) Responsivity measurements are carried out on a single pixel (#15) by initially maximizing the counts with position settings in *x*, *y*, and *z* (see Fig. 1a).

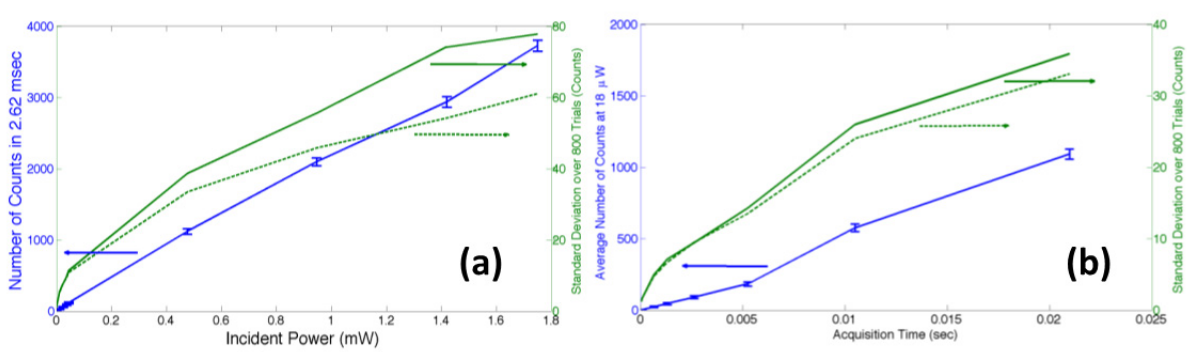

Fig. 3(a) Increase in total counts observed on pixel 15 in 2.62 msec (left) averaged over 800 trials vs. incident power with error bars for 800 trials. (Right) Standard deviation increase as a function of power (solid green curve). Dashed green curve - theoretical standard deviation of a Poisson distribution with same mean as observed number of counts (left). (b) Increase in total counts (left) observed on pixel 15 with 18 µW incident power as the acquisition time interval increases from 41 µsec - 25 msec with error bars over 800 trials. (Right) Standard deviation increase as a function acquisition time (solid green curve). Dashed green curve - theoretical standard deviation of a Poisson distribution same mean as the average number of counts in each acquisition time interval.

To observe the distribution of generated pulses for this process, Fig. 3a, shows the standard deviation over 800 trials (solid green curve) on the right vertical axis. The standard deviation is also depicted as error bars on the average total

counts (blue curve). We note that the standard deviation increases with incident power and total counts. This is expected for a Poisson distribution with mean and variance equal to μ. However, when plotting the expected standard deviation $\sqrt{\mu}$ (dashed green curve), where μ is taken to be the observed average counts (blue curve), the observed standard deviation is roughly equal to $\sqrt{\mu}$ below 45 μW, but begins to exceed this value as the power increases. The increasing difference between the solid and dashed green curves along with incident power is attributable to blocking losses. As we will show, the observed count rate $\mu_{observed}$ is not a Poisson distributed random variable, but is related to the Poisson distributed photoelectron generation rate μ_{actual}. Because of the detector's finite recovery time, a portion of the total photoelectrons generated will not be observed and $\mu_{observed} < \mu_{actual}$. Therefore, we expect the variance of $\mu_{observed}$ to exceed $\sqrt{\mu_{observed}}$.

A Poisson distribution can also be confirmed in the total number of occurrences within a given time interval. In Fig. 3b, the power is fixed at 18 μW and the acquisition time is varied between 41 μsec to 25 msec. Plotting the total number of counts (blue curve) observed over 800 trials for each acquisition time with error bars indicates the standard deviation over these trials. Here we also observe a linear increase in the counts with increasing time interval. The standard deviation (solid green curve) is shown to agree closely with the theoretical standard deviation for a Poisson distribution (dashed green curve) when the acquisition time is below 2.62 msec, but begins to exceed this value at an increasing rate for longer acquisition times. While we do not expect an increased variance with longer acquisition times, this results may be explained due to environmental changes. The data for the shorter acquisition intervals can be transferred between the logic analyzer and PC within a few minutes, while the longer time intervals require ~1 hr. It is possible within this longer period of maintaining light on the laser that temperature variations on the detector or environment would introduce greater uncertainty over longer times.

To observe the actual distribution of counts more directly, we plot histograms of the total counts in 800 trials in Fig. 4a – c. In Fig. 4a, the laser is turned off and only dark counts are observed. In this case, the distribution closely resembles a Poisson fit. For incident power of 25.96 μW, the histogram in Fig. 4b shows that the counts are again Poisson distributed. Because μ is large, the Poisson distribution closely matches a Gaussian distribution as expected. Finally, in Fig. 4c, the count distribution can be fit to a Gaussian with significant differences from the Poisson distribution with the same mean. This is due to the increase standard deviation we observed in Fig. 3a which serves to broaden the distribution curve because of blocking losses as explained above. Nevertheless, our results indicate that the counts can be expected to adhere to either a Poisson below ~ 30 μW or Gaussian distribution at higher power levels, which would facilitate modeling of the expected count rate.

We have recorded the inter-arrival times for incident powers of 0.36 mW, 0.73 mW, and 1.46 mW, and found recovery times to be 30 – 40 nsec for the quenching circuit. In Fig. 5a-b, we have plotted inter-arrival time histograms on a log scale obtained for these three power levels. Figure 5a shows a linear slope as expected for exponentially distributed inter-arrival times. However, there are apparent peaks for small inter-arrival times indicative of afterpulsing[9].

increase in count rate with incident power for four trials (blue curves). In trials 3 and 4, the count rate was maximized at high incident power by adjusting the *xy* and *z* positions. The beam is focused tightly on the detector in these trials, while it is slightly unfocused in trials 1 and 2. The corresponding red curves show the quadratic fits to the data having equations $aP^2 + bP + c$, where P is the incident power. The fits match the data closely at incident powers below ~2 mW. It is apparent from trial 4 (dotted curve) that the detector saturates for higher powers, corresponding to count rates of ~800 KHz and greater. A maximum count rate of 1.32 MHz is observed in trial 4, after which, the count rate begins to decline due to saturation. This prevents us from observing the quadratic response at higher powers, where it is expected to dominate. In Fig. 6c, we plot the expected observed count rates ($\mu_{observed}$) assuming a higher actual photoelectron generation rate (μ_{actual}). This difference is due to blocking losses incurred because any photoelectrons generated within the recovery time of the active quenching circuit will not be observed. The figure shows the relationship between these two quantities assuming that the photoelectrons are Poisson distributed. For a recovery time of 300 ns, the maximum observed count rate is 1.22 MHz (red curve). This agrees with the maximum we have measured on the single photon detector. We note that although the detector's maximum pulse rate could be as high as 3.33 MHz, we only observe count rates up to 1.22 MHz due to photon bunching. Smaller photon inter-arrival times are more probable than longer ones as illustrated in Fig. 5. As a result, a significant portion of photoelectrons are generated within the recovery time and cannot be observed. The maximum observable count rate is related to the recovery time by

$\mu_{observed}^{max} = 1/e\, T_{recovery}^{min}$. For comparison, given a 30 ns recovery time as observed on the 6 x 6 array, the plot for $\mu_{observed}$ in Fig. 6c (blue curve) is nearly linear in the region of interest and blocking losses are approximately 15%.

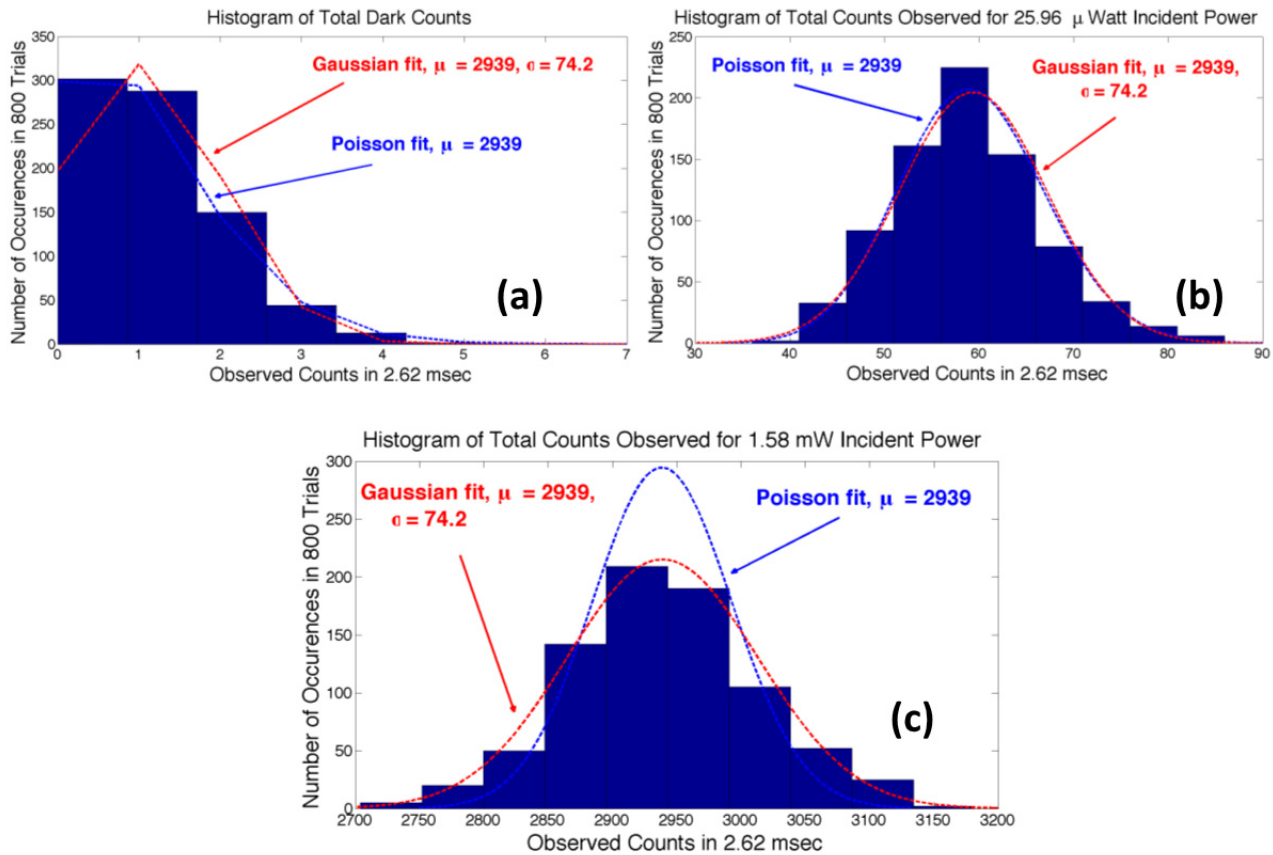

Fig. 4 Histograms of total counts observed in 2.62 msec over 800 trials with (a) no power, (b) 26 μW incident power, and (c) 1.58 mW incident power. Red and blue dashed curves indicate corresponding Gaussian and Poisson distribution fits respectively.

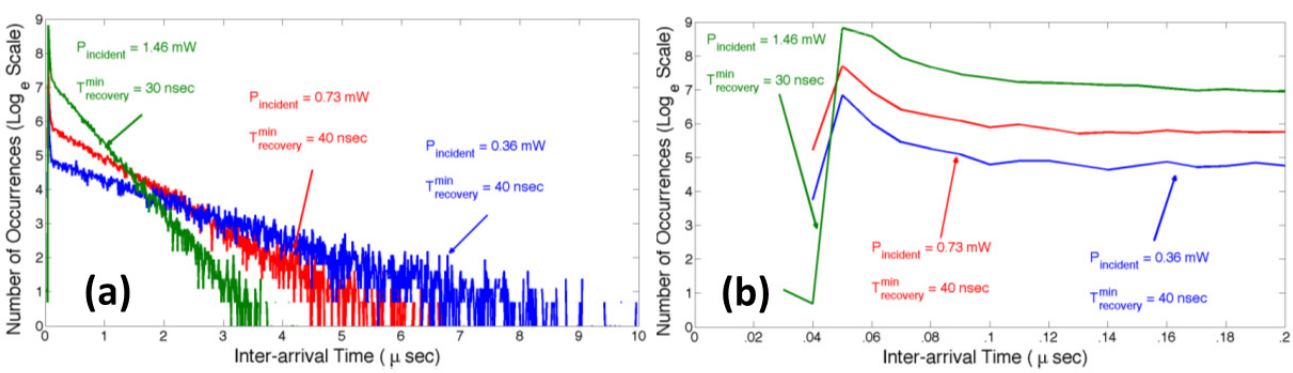

Fig. 5 (a) Inter-arrival time distributions plotted on a log scale for 3 different incident powers on a single pixel in the 6 x 6 array. (b) Same data as in (a) but magnified around smaller times to highlight the observed minimum recovery time and afterpulsing.

We have also measured the count rate with increasing power on a silicon single pixel photon counting module with passive quenching circuit. The output pulses are 100 ns long, and we have observed a recovery time of approximately 300 ns. Therefore, we expect this detector's maximum pulse rate to be 3.33 MHz. Figure 6 (a) plots the measured
The strength of both the linear and quadratic responses is shown to vary over different trials. The coefficients a and b all increase for trials 3 and 4 compared to trials 1 and 2. A precisely focused beam is expected to increase the strength of the two-photon quadratic response, but our data shows that it is also increasing the strength of the linear absorption. We have previously observed this effect on our 6 x 6 Geiger mode array. Indeed, comparing the ratio of coefficients $\frac{b}{a}$ = 6.8, 5.8, 3.6, 7.2 for trials 1-4 respectively. Although $\frac{b}{a}$ for trial 4 is larger than for trials 1 and 2, $\frac{b}{a}$ is smaller for trial 3 than for trial 1 and 2. We can infer from this that focusing the beam appear to increase the strength of both the linear and quadratic response, and in some cases benefit the linear response to a greater extent than the quadratic one. It is possible that the observed increased strength of the linear response occurs because the beam is centered on the microlenses, allowing the maximum amount of light to focus on the detector. The sensitivity of the sub-band absorption to position in x, y, and z was observed on the Geiger mode array, and confirmed on our single pixel photon counting module.

Figure 6 (b) presents the detection efficiency measured over the four trials. The detection efficiency is greatest at low powers with a maximum observed value of $\sim 1.2x10^{-10}\ counts/photon$, consistent with that measured on the Geiger mode detector array ($1.01x10^{-10}\ counts/photon$). The responsivity reported in Ref. [8] was 10^{-9} - 10^{-8} A/W for a PIN detector below 10 mW of incident power. A corresponding value for our photon-counting detectors is obtained by multiplying the number of counts by $1.6x10^{-19}$ Coulombs, the charge of a single electron, which estimates the equivalent number of photocarriers generated in the Geiger mode detector. This gives an equivalent photocurrent for comparison with the PIN detector equal to $1.24x10^{-10}$ A/W. Evidently, the responsivity is 1 – 2 orders of magnitude lower for our photon-counting detectors than for a PIN. Photon counting detectors are typically fabricated with thinner absorption layers in order to reduce the dark noise[11-13], which may account for the observed difference in responsivity.

3. CONCLUSION

We confirmed that sub-band absorption is observable on a silicon Geiger-mode detector array by placing the detector at the focal point of the laser beam. We observed a detection efficiency over 60 dB below that of previously measured single-photon response on the same detector, which proves the validity of the DOT design concept for isolation. Our measurements demonstrate that such a design would feasibly track of two laser beams of different wavelengths on the same detector array simultaneously via two different physical absorption processes.

Two photon absorption is characterized by a linear dependence of responsivity on incident power, whereas we have observed a nearly constant detector responsivity, based on the number of registered counts produced by the active quenching circuit on our Geiger mode array. In addition, our measurements on a single pixel photon counting module confirmed the existence of this linear sub-band absorption process, along with a quadratic component from the two-photon absorption. As expected, the non-linear two-photon absorption begins to dominate as the power is increased. Nevertheless, the linear sub-band absorption is an interesting finding, which has been previously observed at low powers on a silicon PIN detector. Our results for the responsivity at 1550 nm of two active quenching modules were 10-20 dB lower than the PIN detector.

The distribution of counts for our 6 x 6 Geiger mode array has greater standard deviation than a theoretical Poisson distribution, attributable to blocking loss. However, we showed that the data can be modeled with familiar Poisson and Gaussian distributions in low and high power regimes respectively.

To accurately model the distribution of counts, the role of the active quenching circuit in controlling the detector overbias must be understood in greater depth, and a model that includes blocking losses[14], detection efficiency, afterpulsing, saturation, dark, and excess noise must be developed. In addition, the reflectivity, shape, and aberrations of the microlenses must be carefully included in our model to accurately account for the complex scattering mechanisms they introduce among different pixels. Tilting, alignment, and foucs of the detector must also be controlled to enable reliable measurements.

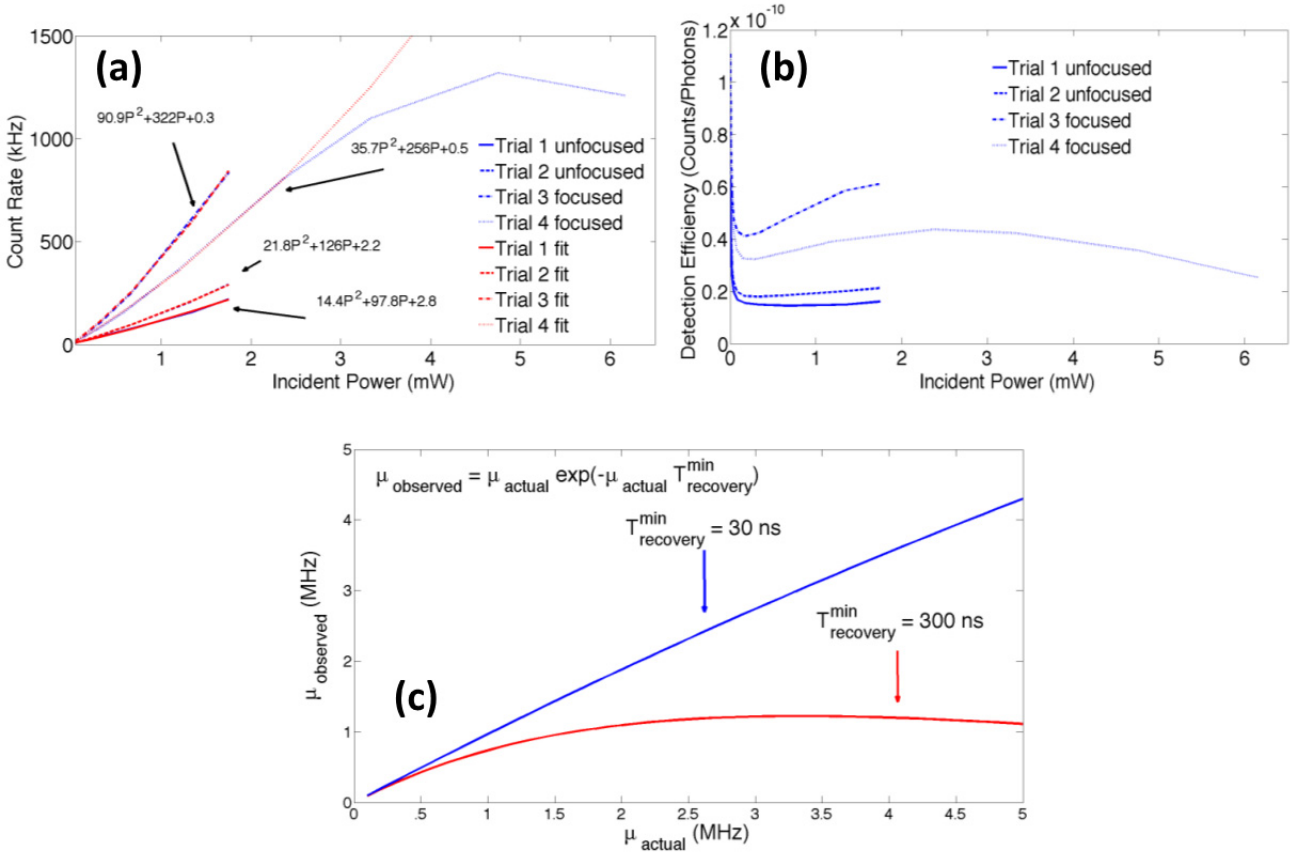

Fig. 6 (a) Measured count rate vs. incident power on silicon single pixel photon counting module. Trials 1 and 2 (blue solid and dashed curves respectively) represent measurements taken with the beam off focus. For trials 3 and 4 (blue dot-dash and dotted curves respectively), the focus was adjusted to maximize the counts at high powers. Corresponding red curves show quadratic curve fits performed for all trials and the resulting equations are given as labels. (b) Calculated detection efficiency in counts/photons vs. incident power for the four trials given in (a). (c) Calculated observed counts vs. actual counts due to blocking loss given a recovery time of 300 ns (red curve) for our single pixel detector, and 30 ns (blue curve) observed for our 6 x 6 array.

ACKNOWLEDGMENTS

This research was carried out at the Jet Propulsion Laboratory, California Institute of Technology, under a contract with the National Aeronautics and Space Administration.

REFERENCES

[1] Hemmati, H., [Deep Space Optical Communications], John Wiley & Sons Inc., Hoboken, New Jersey, 16-355 (2006).

[2] Hemmati, H., Farr, W. H., Biswas, A., Birnbaum, K. M., Roberts, W. T., "Deep-space optical terminals (DOT)," Proc. SPIE, 7923 (79230C) (2011).

[3] Farr, W., Sburlan, S., Sahasrabudhe, A., Birnbaum, K., "Deep space acquisition and tracking with single photon detector arrays," Proc. IEEE, Proc. ICSOS, *To be published*, (2011).

[4] Sburlan S., Farr. W., Birnbaum, K., “Deep space space uplink receiver prototype for optical communications,” Proc. SPIE, 7923 (79230K) (2001).
[5] Ortiz, G., Farr, W. H., Charles, J. R., Roberts, W. T., Sannibale, V., Gin, J., Saharabhude, A., Garkanian, V., “Canonical deep space optical communications transceiver,” Proc. SPIE, 7199 (71990K) (2009).
[6] Nakanishi, T., Kobayashi, H., Sugyiyama, K., Kitano, M., “Full quantum analysis of two-photon absorption using two-photon wave function: comparison of two-photon absorption with one-photon absorption,” J. Phys. Soc. Jpn. 78 (104401) (2009).
[7] Biswas, A., Hemmati, H., Piazzolla, S., Moision, B., Birnbaum, K. M., Quirk, K., “Deep-space optical terminals (DOT) systems engineering,” Interplanetary Network Progress Report, 42-183 (2010).
[8] Ortiz, G. G. and W. H. Farr, “Two-photon absorption long-wavelength optical beam tracking,” IPN PR 42 (173), 1, (2008).
[9] Jiang, X., Itzler, M., Ben-Michael, R., Slomkowski, K., Krainak, M. A., Wu, S., Sun, X., “Afterpulsing effects in free-running InGaAsP single-photon avalanche diodes,” IEEE J. Sel. Topics QE, 44 (1), 3 (2008).
[10] Jiang, X., Itzler, A., Ben-Michael, R., Slomkowski, K., “InGaAsP-InP avalanche photodiodes for single photon detection,” IEEE J. Sel. Topics QE, 13 (4), 895-905 (2007).
[11] Donnelly, J., Duerr, E., McIntosh, K. A., Dauler, E. A., Oakley, D. C., Groves, S. H., Vineis, C. J., Mahoney, L. J., Molvar, K. M., Hopman, P. I., Jensen, K. E., Smith, G. M., Verghese, S., Shaver, D. C., “Design considerations for 1.06-μm InGaAsP-InP Geiger-mode avalanche photodiodes,” IEEE J. Sel. Topics QE, 42 (8), 797 (2006).
[12] Pellegrini, S., Warburton, R. E., Lionel, J. J. T., Ng, J. S., Krysa, A. B., Groom, K., David, J. P. R., Cova, S., Robertson, M., Buller, G. S., “Design and performance of an InGaAs-InP single-photon avalanche diode detector,” IEEE J. Sel. Topics QE, 42 (4), 397 (2006).
[13] Itzler, M. A., Ben-Michael, R., Hsu, C. F., Slomkowski, K., Tosi, A., Cova, S., Zappa, F., Ispasoiu, R., “Single photon avalanche diodes (SPAD) for 1.5 μm photon counting applications,” J. Modern Optics, 54 (2-3), 283 (2007).
[14] Moision, B., Piazzolla, S., “Blocking losses on an optical communications link,” IEEE, Proc. ICSOS, *To be published*, (2011).